The Astrophysical Journal Letters, 942:L3 (8pp), 2023 January 1 https://doi.org/10.3847/2041-8213/aca97c

Magnetic Outbreak Associated with Exploding Granulations

Chunlan Jin[1], Guiping Zhou[1], Guiping Ruan[2], T. Baildon[3,4], Wenda Cao[3,4], and Jingxiu Wang[1,5]
[1] Key Laboratory of Solar Activity and Space Weather, National Astronomical Observatories, Chinese Academy of Science, Beijing 100101, People's Republic of China; cljin@nao.cas.cn
[2] Shandong Provincial Key Laboratory of Optical Astronomy and Solar-Terrestrial Environment, and Institute of Space Sciences, Shandong University, Weihai 264209, People's Republic of China
[3] Center for Solar-Terrestrial Research, New Jersey Institute of Technology, 323 Martin Luther King Blvd, Newark, NJ 07102, USA
[4] Big Bear Solar Observatory, 40386 North Shore Lane, Big Bear City, CA 92314, USA
[5] School of Astronomy and Space Science, University of Chinese Academy of Sciences, 100049, Beijing, People's Republic of China
Received 2022 July 31; revised 2022 December 7; accepted 2022 December 7; published 2022 December 27

Abstract

Diagnosing the spatiotemporal pattern of magnetic flux on the Sun is vital for understanding the origin of solar magnetism and activity. Here, we report a new form of flux appearance, magnetic outbreak, using observations with an extremely high spatial resolution of 0.″16 from the 1.6 m Goode Solar Telescope at the Big Bear Solar Observatory. Magnetic outbreak refers to an early growth of unipolar magnetic flux and its later explosion into fragments, in association with plasma upflow and exploding granulations; each individual fragment has flux of 10^{16}–10^{17} Mx, moving apart with a velocity of 0.5–2.2 km s^{-1}. The magnetic outbreak takes place in the hecto-Gauss region of pore moats. In this study, we identify six events of magnetic outbreak during 6 hr observations over an approximately $40'' \times 40''$ field of view. The newly discovered magnetic outbreak might be the first evidence of the long-anticipated convective blowup.

Unified Astronomy Thesaurus concepts: Solar magnetic fields (1503); Solar photosphere (1518); Solar granulation (1498); Solar activity (1475)

Supporting material: animations

1. Introduction

The appearance of magnetic flux on the solar surface manifests a fundamental process that energizes solar atmosphere and leads to solar eruptions (e.g., Magara & Longcope 2003; Guglielmino et al. 2010). Flux appearance signifies the physical interaction between plasma motion and the generated magnetic fields. For the past century, observations have shown that magnetic flux emerges in a bipolar form on the Sun, from the strong-field regime, e.g., in active regions (ARs), to the weak-field regime, and even in internetwork (IN) regions (Schrijver & Zwaan 2000; Cheung et al. 2010; Stein et al. 2011; Wang et al. 2012). However, an exception to this is moving magnetic features (MMFs), which have drawn intense attention in the solar physics community (Sheeley 1969; Harvey & Harvey 1973). MMFs do not typically exhibit the evolutionary pattern of an emerging flux region, i.e., the systematic growth and separation of opposite polarities, although Type I MMFs do appear in bipoles (Wilson 1986; Spruit et al. 1987; Thomas et al. 2002; Zhang et al. 2003). Type II and Type III MMFs, however, are unipolar magnetic features (Shine & Title 2000).

In the past few years, a number of small-scale flux-emergence events occurring at mesogranular and granular scales have been studied. Observations show that exploding granules (EGs) are associated with flux emergence occurring at mesogranular scale (Guglielmino et al. 2020), and contributes to organize the discrete magnetic field (e.g., Roudier et al. 2016; Malherbe et al. 2018; Roudier et al. 2020). Granule-covering magnetic sheet-like structures in the quiet Sun have been found by observations (Centeno et al. 2017; Fischer et al. 2019) and numerical simulations (Moreno-Insertis et al. 2018). Furthermore, the appearance of unipolar features in IN flux has been observed (Gošić et al. 2022).

Based on magnetic observations with extremely high spatial resolution, we find a new magnetic phenomenon with unipolar form: magnetic outbreak. This phenomenon is found in pore moats—the same magnetic environment as MMFs. In this paper, we will present our new findings in detail. Observations and data analysis are presented in Section 2, and in Section 3 we give a detailed description of the magnetic outbreak phenomenon. We discuss our findings in the context of previous research and provide some possibilities to explain the new observation in Section 4. Finally, conclusions are made in Section 5.

2. Observations and Data Analysis

Extremely high-spatial-resolution observations of NOAA AR 12579 on 2016 August 25 were achieved by the 1.6 m Goode Solar Telescope (GST; Goode & Cao 2012; Cao et al. 2010). The observations were made with the Near InfraRed Imaging Spectropolarimeter (NIRIS; Cao et al. 2012, 2022) over the 1.56 μm Fe I line at the Big Bear Solar Observatory (BBSO), and have high spatiotemporal resolution: approximately 57 km pixel^{-1} and 41 s cadence. NIRIS produces full spectropolarimetric measurements I, Q, U, and V (Stokes profiles) at a spectral resolution of 0.01 nm, with a typical range of −0.32 nm to +0.31 nm from the line center. Broadband TiO images centralized at 705.7 nm were obtained with a high spatial resolution of 25 km pixel^{-1} and temporal resolution of 15 s at BBSO. Images and magnetograms from the Solar

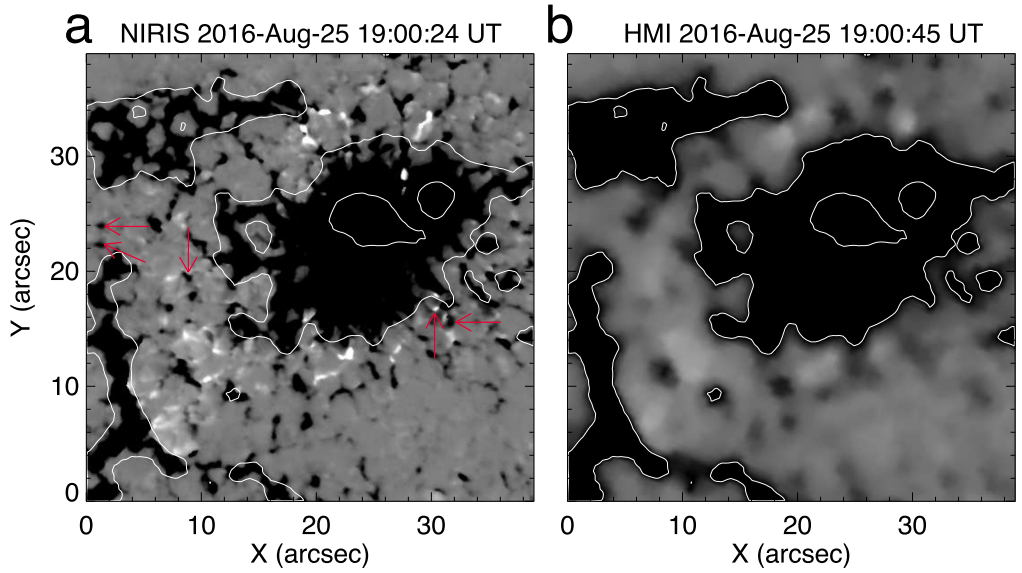

Figure 1. Comparison of magnetic observations between NIRIS and HMI. The line-of-sight magnetic observations from NIRIS (a) and HMI (b) were taken on 2016 August 25 at 19:00 UT. The magnetic field saturates at ±100 G. Large-scale structures are outlined in white in both images.

Dynamics Observatory (SDO; Pesnell et al. 2012) were also used for coordinative data analysis.

Each NIRIS data sample (pixel) is comprised of Stokes profiles taken at 55 spectral points. The rms fluctuation of the spectral continuum is 0.11% in the Stokes Q and U spectra, and 0.09% in the Stokes V spectrum. The NIRIS data undergo Stokes inversion based on the Milne–Eddington atmospheric model (Ahn et al. 2016), through which several physical parameters, including vector magnetic field and Doppler shift, have been obtained. A magnetic signal as low as 4 G can be detected for the line-of-sight field. The accuracy of the resulted vector field data reaches 10 G for the line-of-sight component and 100 G for the transverse component (Wang et al. 2017). In addition, the inverted Doppler velocity is calibrated by setting the average Doppler velocity of the very quiet region to be zero.

The NIRIS line-of-sight magnetic observations are compared with magnetic measurements from the Helioseismic and Magnetic Imager (HMI; Scherrer et al. 2012) instrument onboard SDO. HMI enables magnetic observations with a pixel size of 362 km and cadence of 45 s. The compared magnetograms are shown in Figure 1. We can see a similarity in the larger-scale magnetic structures between the NIRIS and HMI magnetograms, and more fine-scale structures in NIRIS magnetic observations due to higher spatial resolution. We further compare the magnetic flux of the main magnetic structures, which are outlined in white in Figure 1, and obtain a flux measurement ratio of 1.2 between NIRIS and HMI. A few magnetic elements, indicated by arrows in the NIRIS magnetogram, are completely missing in the HMI magnetogram. This illustrates the advantage of using NIRIS observations for exploring small-scale magnetic evolution on the solar surface (Wang et al. 2017), and small-scale magnetic structures can only be revealed via high spatial resolution (Jin & Wang 2019).

3. Magnetic Outbreak Phenomenon

Approximately 6 hr continuous observations from 16:36 UT to 22:16 UT were taken of the negative polarity region of AR 12579. The negative magnetic region mainly consists of two pores, indicated by the black arrows in Figure 2(b). We identify six events of magnetic outbreak during the observations; the locations of these events are distributed in the moats of pores, which are framed in Figures 2(a) and (b). The primary properties of the magnetic outbreaks are listed in Table 1. In this table, the foreshortening effect may affect the values of the line-of-sight magnetic component, because the observation is not acquired at the disk center. However, considering the quieter magnetic environment of these outbreak events and the larger errors from the transverse field, the foreshortening effect is not corrected in this study.

Event 1 (labeled "1" in Figure 2) is a typical event of magnetic outbreak with relatively longer duration and larger magnetic flux, and thus is worthy of a detailed discussion. Event 1 takes place in a cell region of mesogranular size (November et al. 1981). The process of magnetic outbreak consists of three phases: the growing phase, the exploding phase, and the fading phase, all of which are shown in Figure 3. The detailed evolution within the three phases is described below.

1. *The growing phase.* Starting around 19:50 UT, a lump of positive magnetic flux appears and grows, reaching a maximum flux density of 107 G at about 20:02 UT. This growing phase is characterized by the rapid increase of both total flux and flux density (see Figure 4). In this period, the positive flux keeps its center position unchanged (see Figure 3), while its area expands. The flux gradually increases to 1.1×10^{19} Mx at about 20:04 UT; meanwhile there is no corresponding increase of negative flux (see Figure 4). Furthermore, the transverse field emerges and develops in this period, and its density reaches 317 G around 20:02 UT, which reveals a highly inclined field of the event (see Figure 5). The growth of positive flux is accompanied by concentrated blueshifts in NIRIS Dopplergrams, indicating an updraft of -0.1 km s^{-1} (see Figure 5). Moreover, an EG (Musman 1972; Rempel 2018; Roudier et al. 2020; Guglielmino et al. 2020) appears around 20:00 UT, right after the

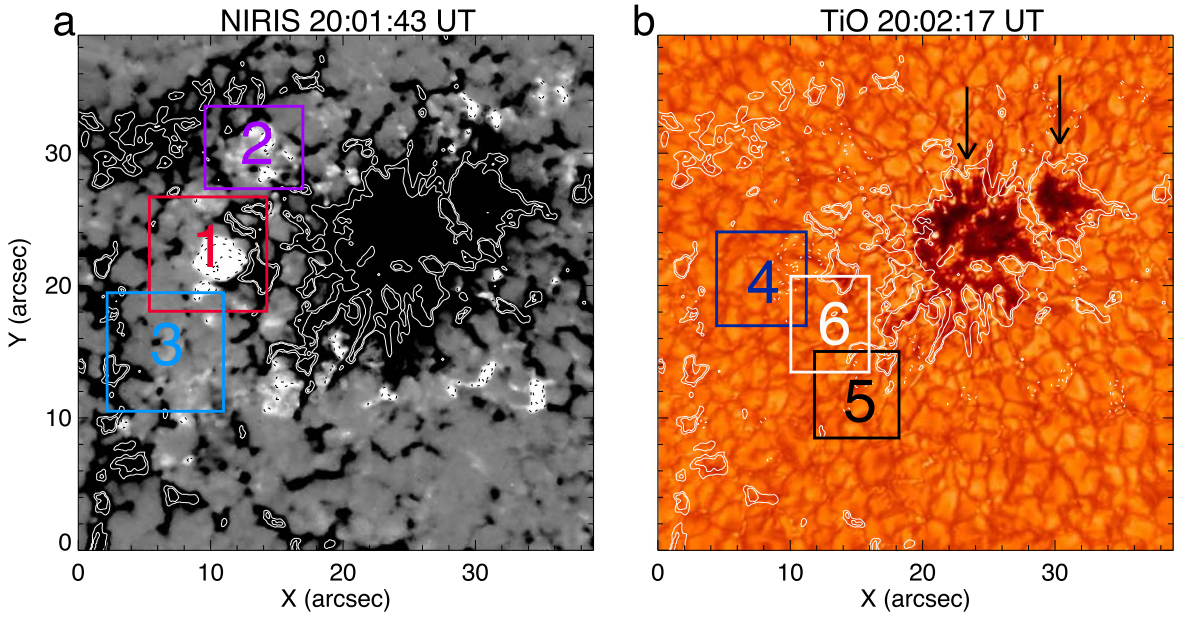

Figure 2. The magnetic environment of magnetic outbreak events. The positions of outbreak events are indicated in the NIRIS magnetograms (scaled between ±50 G) (a) and TiO image (b). The six events appear in the moats of pores. The solid and dotted contour lines correspond to negative and positive magnetic field values of [−1000 G, −300 G, 50 G, 200 G].

Table 1
Fundamental Properties of the Six Observed Magnetic Outbreak Events

Event No.	Appearing Time (UT)	Maxflux Time (UT)	Ending Time (UT)	Lifetime (min)	Flux (Mx)	LOS Field[a] (G)	Transverse Field[a] (G)	Velocity[b] (km s^{-1})
1	19:50	20:04	21:16	86	1.1e19	107	317	1.3/0.7
2	19:30	19:43	20:27	57	3.0e18	85	245	0.6/0.8
3	21:27	21:54	after 22:16		1.2e19	60	172	1.2/0.5
4	17:58	18:21	18:57	64	5.3e18	68	180	1.1/0.5
5	19:43	19:48	20:15	32	1.4e18	40	151	2.2/0.6
6	20:41	21:00	21:58	77	3.4e18	50	199	0.5/0.9

Notes.
[a] Both line-of-sight field and transverse field mean the magnetic flux density of outbreak events.
[b] The velocity is obtained by two methods, i.e., a time slit of the magnetogram and Fourier local correlation tracking (FLCT). A continuous observation, during which the exploding phase occurs, is adopted to obtain the velocity based on the FLCT method. The used field of views for FLCT are labeled by square frames in Figure 2 for the six outbreak events.

early flux growth. The EG grows to mesogranulation scale at approximately 20:08 UT; another EG then appears in the dark notch of the former (shown by the "+" in Figure 5). In this growth period, transient brightening is found in the upper photosphere, but there is no obvious response in the chromosphere (see Figure 5).

2. *The exploding phase.* Around 20:12 UT, the positive flux begins to split into many fragments which move apart with an average velocity of 1.3 km s^{-1}, looking like an exploding bomb (see Figure 3). Furthermore, the velocity distribution acquired by the Fourier local correlation tracking (FLCT; Fisher & Welsch 2008) method also displays the exploding property, which is shown in the bottom panel of Figure 4. Here, the width σ of the Gaussian windowing function for the FLCT method adopts a 15 px size, i.e., 1.2″. At about 20:34 UT, the main explosion completes, and the positive flux fragments can be seen marking the explosion fronts, while we also see ordinary granulations and calming of plasma upflows (see Figure 5). In this process, the flux density and magnetic flux of the positive flux gradually decreases (see Figure 4). Interestingly, a secondary or subsequent outbreak is observed in a subset window (framed in Figure 3(k)), and its explosion fronts are outlined by exploding fragments of the positive flux. For this secondary outbreak, the total flux reaches a maximum of 1.5×10^{18} Mx at about 20:43 UT (see Figure 4). The same type of secondary magnetic outbreak is also observed in Event 2.
3. *The fading phase.* The process lasts until 21:16 UT, when all the flux fragments in the primary and secondary outbreaks disappear. These explosion fragments either cancel with the surrounding negative field or diffuse to levels below the magnetic noise.

We refer to the whole process—from the first appearance of unipolar positive flux to the disappearance of the exploding fragments—as "magnetic outbreak" in this study. We note that the ambient enhanced network is forced to decay and move farther from the pores during magnetic outbreak (see Figure 3).

Only for the third among the six events are observations truncated due to bad weather during the late fading phase. All of the magnetic outbreak events take place in the moats of pores,

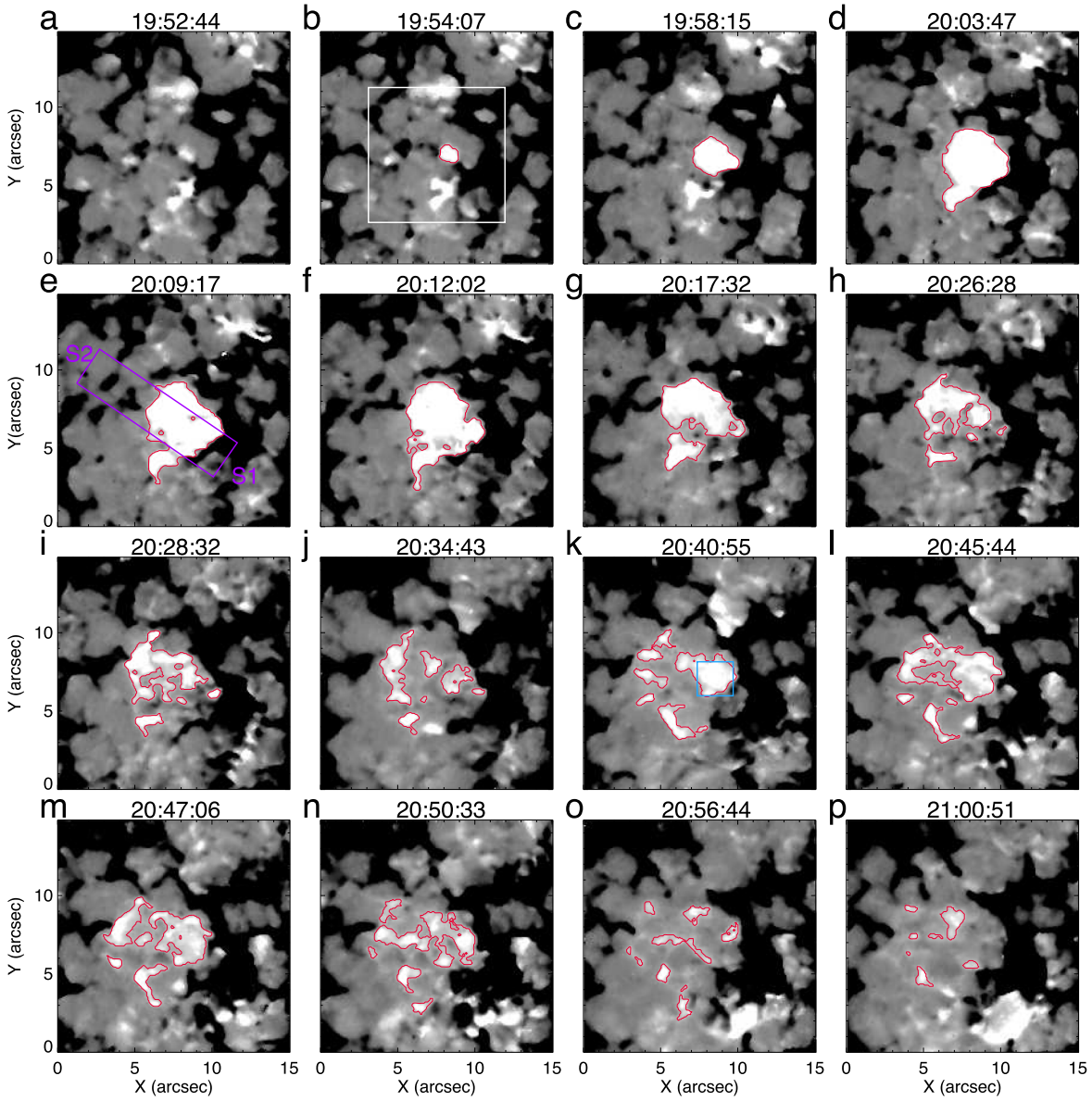

Figure 3. Time series of NIRIS magnetograms (scaled between ±50 G) showing the process of outbreak Event 1. The outbreak flux patches are outlined in red. The magnetic field framed in blue in (k) indicates the secondary outbreak. The slit S1–S2 in (e) is used to obtain the velocity of magnetic outbreak patches. The area framed in the white box in (b) has the same field of view as the red box in (a) of Figure 2. An animation of this figure is available. The animation lasts 4 s and covers 1.45 hr of solar time from 2016 August 25 at 19:48 UT. As a comparison, the corresponding HMI magnetic evolution is also available in the animation.

(An animation of this figure is available.)

and they share a few key properties: (1) appearance of unipolar positive magnetic flux with hecto-Gauss flux density, which is accompanied by plasma upflow; (2) increase in both magnetic flux and flux density during the positive flux growth, without in-phase changes of negative flux; (3) eruption of EGs during the flux growing and exploding phases; and (4) weak transient brightening appearing at the border between the positive flux and the enhanced negative network in the upper photosphere, without chromospheric correspondence in radiation.

4. Discussion

4.1. The Resemblances and Differences of Magnetic Outbreak with Previous Findings

Magnetic outbreak displays many similarities with MMFs, in view of its relation to pore/spot moats, spatial size, flux level, and moving velocity. It is worth noting that the nonuniform magnetic explosion results in an apparent outflow of flux elements in the moat, which can be seen in lower-resolution observations. We see Event 1 in the time sequence of 1″–2″ resolution HMI magnetograms (see Figure 3, animation), which looks like Type III MMFs, i.e., outflowing magnetic features with polarity opposite to the parent pore. On the other hand, in the GST/NIRIS magnetograms many Type III MMFs are observed, but they never exhibit an exploding nature (Li et al. 2019). Therefore, magnetic outbreak seems not to fit the scenario of MMFs.

We carefully checked the magnetic and velocity observations, and considered all the possibilities, in particular whether or not the observations fit in an already known "family" in the published literature, e.g., Moreno-Insertis et al. (2018), Guglielmino et al. (2020), Roudier et al. (2020), etc. The

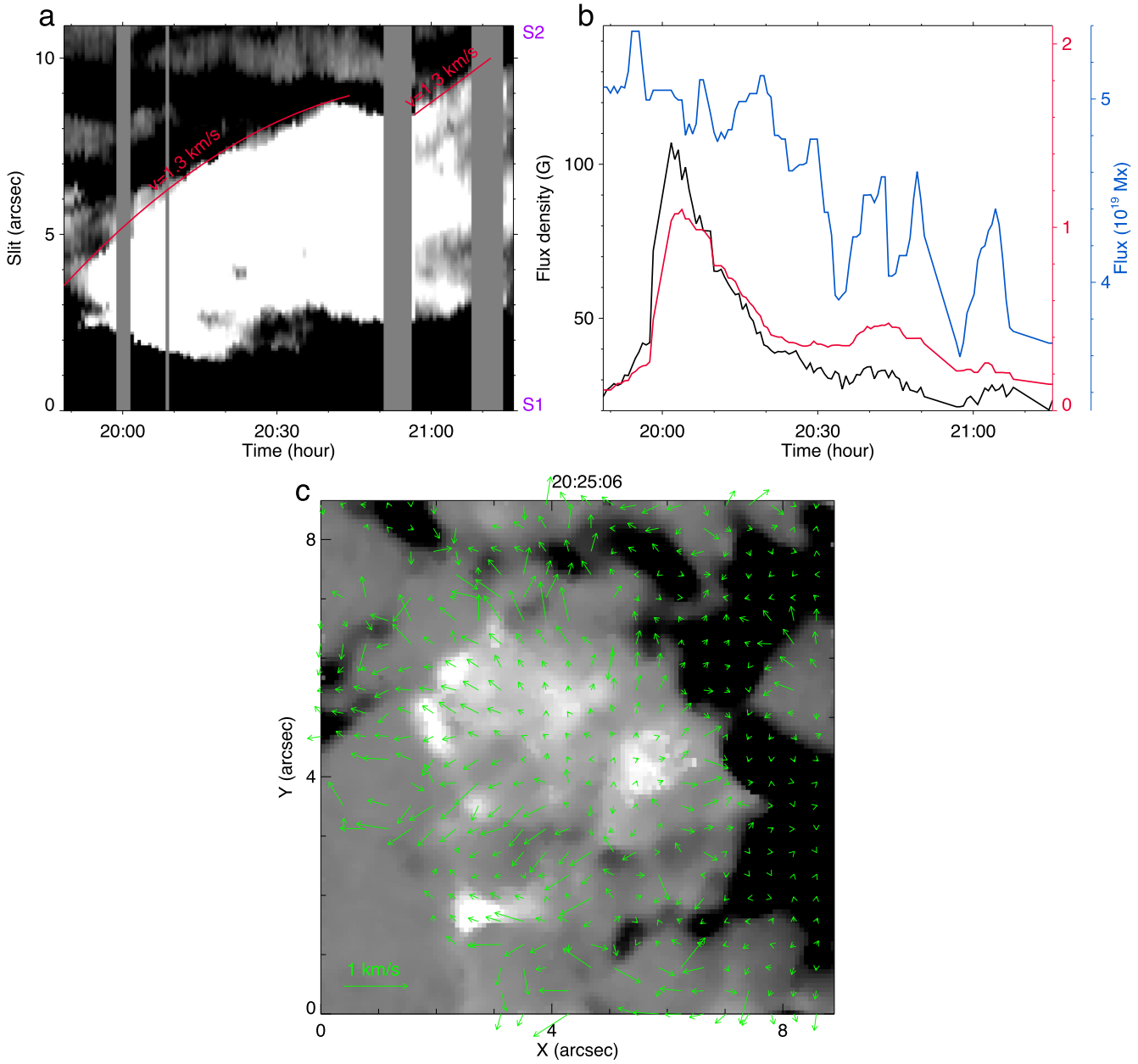

Figure 4. Top panels: the time slit and magnetic variation for Event 1. (a) The time series of the slit in Figure 3(e). This data is used to estimate the exploding velocity. Gray regions denote missing observations. An average velocity of 1.3 km s^{-1} is obtained by the fitting. (b) Magnetic variations in the domain framed in white in Figure 3(b) are plotted for the flux density (black line) and flux (red line) of the magnetic outbreak, as well as the magnetic flux of the negative field (blue line). Bottom panel: the velocity distribution for Event 1, ranging from 20:10 UT to 20:50 UT, which is obtained by the FLCT method in a 9″ × 9″ sub-FOV. Event 1 is centered on (5″, 5″), and its average velocity is 0.7 km s^{-1}.

answer is not exactly. First, the magnetic outbreak is not a phenomenon within a granule, but takes place in the interior of the enhanced network at mesogranular scale. Plasma upflow plays a role in triggering the EGs and the later magnetic explosion (see the Dopplegrams and granule images in Figure 5), similar to that described by Guglielmino et al. (2020). Second, the magnetic outbreak is not related to IN horizontal elements (Lites et al. 2008). Jin et al. (2009) were the first to classify the IN horizontal elements into two classes: one class associated to a pair of line-of-sight elements, representing a small-scale loop emergence; the other isolated from line-of-sight elements. However, their studied horizontal IN elements do not show eruptive behavior. Third, the field configuration of magnetic outbreak is not like the horizontal flux sheets covering a whole granule by simulation (Moreno-Insertis et al. 2018), and the horizontal sheet emergence followed by basically the bipolar appearance in observation (Fischer et al. 2019). The well-organized inclined fields in outbreak events are manifested by prevailing positive line-of-sight flux and stronger transverse field with connection to the surrounding negative network. Fourth, our observations demonstrate a convective instability initiated with updraft of plasma, which leads to the explosion in the studied magnetic outbreak. In these events, the enhanced network might play some role in penetrating radiation to heat its interior, which initiates the instability. To our knowledge, the convective instability triggered by plasma upward motion has not been previously described in the existing literature.

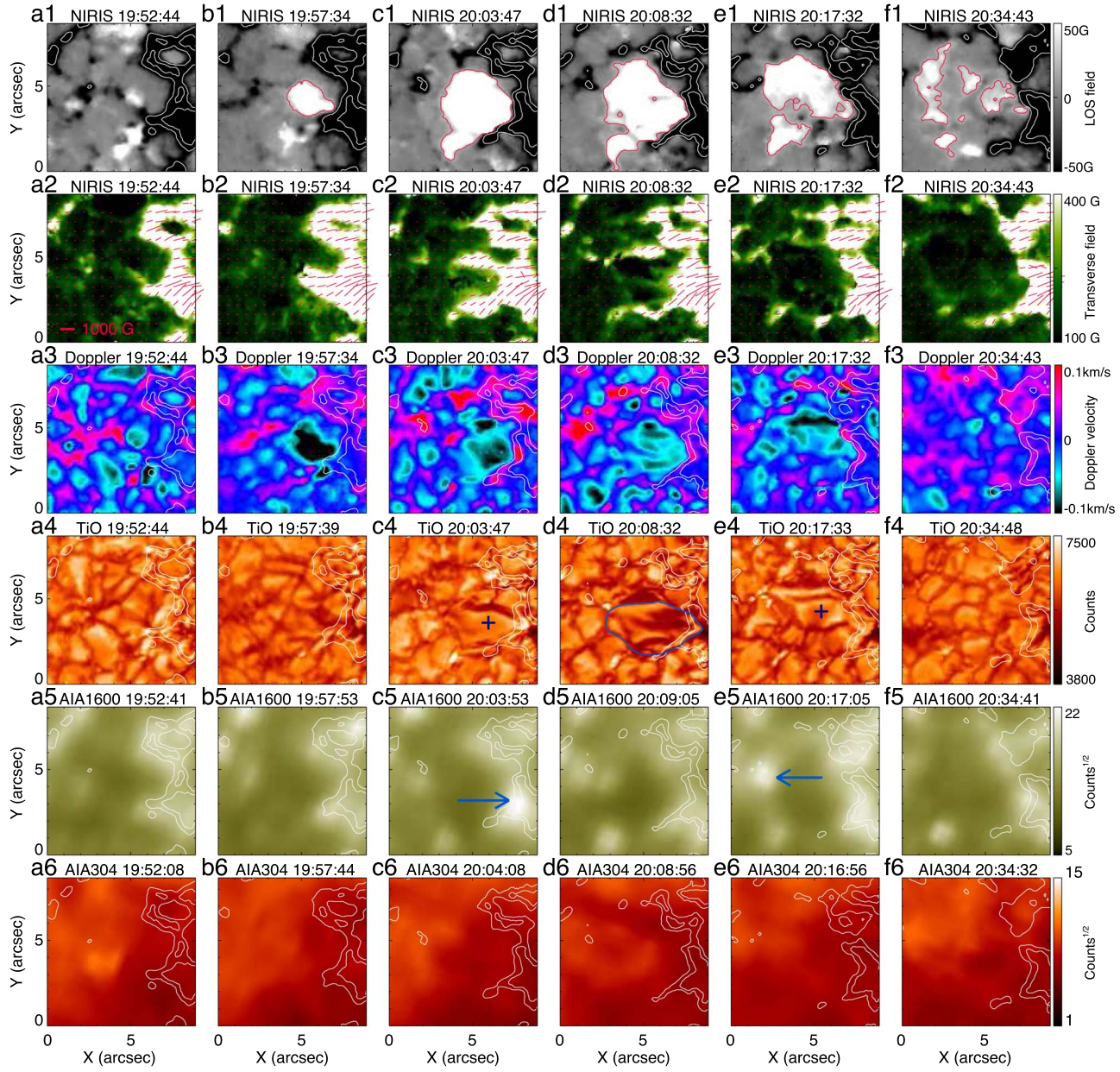

Figure 5. Time series images showing the convection and atmospheric response during Event 1. First row: line-of-sight magnetograms. Second row: transverse magnetograms, where the transverse fields with values larger than 100 G are shown by red lines. Third row: Dopplergram. Fourth row: TiO images. Fifth and sixth rows: AIA 1600 Å and 304 Å images. Contour lines of [−1000 G, −100 G] from synchronous NIRIS line-of-sight magnetograms are marked by the white lines in these images. The field of view (FOV) of these images is the same as that in red in Figure 2. An animation of this figure (including NIRIS line-of-sight field, Doppler velocity, AIA 1600 and AIA 304 images) is available, and these images in the animation are shown by a larger FOV, which is the same as that in Figure 3. The animation lasts 4 s and covers 1.45 hr of solar time from 2016 August 25 at 19:48 UT.

(An animation of this figure is available.)

4.2. How Do We Understand the Observed Magnetic Outbreak?

The observed magnetic outbreak raises several interesting questions, such as: Why do we only see the growth of uniform positive flux? What is the basic magnetic topology which serves as the magnetic outbreak? What physics underlie the observations?

We tentatively propose that the magnetic topology gestated the magnetic outbreak, which could be simplified as a U-loop with an open bottom, as seen in the sketch in Figure 6. The strong vertical field at the network boundary likely connects a reservoir of horizontal field underneath the solar surface at a depth between the bottoms of mesogranulation and supergranulation (Rempel & Cheung 2014; Cheung et al. 2007). The overall magnetic configuration is quite similar to U-loops in the literature (Wilson 1989), except for its open bottom. Penetration from lateral radiation would result in a temperature rise, causing the plasma to flow upward (see Schrijver & Zwaan 2000), which stretches the horizontal magnetic strands. As a net result of many such upstretched field lines, we would see the appearance of equivalent unipolar flux with positive polarity. Moreover, by the tension force of the stretched field, the emergent magnetic flux should be strongly inclined. In other words, one would see the inclined flux with unipolar

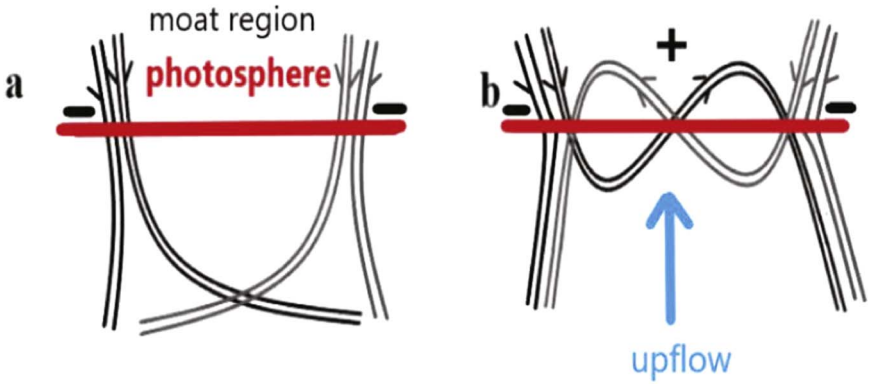

Figure 6. Sketch that may account for the unipolar flux in the observed magnetic outbreak events: drafting by plasma upflow. Red lines indicate the photospheric layer, and the region between the black and gray magnetic lines is the pore moat.

positive flux and strong horizontal field component connecting to the negative network.

In contrast to the well-known convective collapse, as soon as a convective instability occurs in the upflow with the field, the initial updraft would be enhanced and the flux tube would expand. As a result of this increased instability, the flux tube would be torn to shreds and the plasma return to a normal convective state (Spruit & Zweibel 1979; Spruit 1979; Schrijver & Zwaan 2000). The convective blowup of magnetic tubes was predicted more than 40 years ago, but it has never been observed. Observations with the extremely high spatial resolution and good polarization sensitivity from GST might enable us to report the first apparent evidence of convective blowup.

The observed magnetic outbreak has vividly illustrated the generally physical picture of convective blowup. The most striking characteristics in the observed magnetic outbreak are the coinciding plasma upflow and flux explosion. We seem to witness the convective instability in plasma upflow and the real-time blowup of magnetic flux. In addition, observations have shown how the rapid development of plasma upflow results in EGs. The EGs appear to be involved in convective blowup. It is convective instability that conducts the magnetic outbreak.

The identified magnetic outbreak in this study takes place in the fading phase of AR 12579. The six outbreak events have a total flux of about 3.6×10^{19} Mx, which is approximately 11% of the total flux loss in the parent pore region. This is indicative that convective blowup plays a role in the removal of magnetic flux from the pore region. We consider the conjugated convective collapse and blowup to play a key role in shaping the spatiotemporal pattern, followed by vigorous flux emergence and cancelation. The former creates various strong-field structures, and the latter transforms the magnetic flux from the strong-field realm to the weak-field reservoir.

5. Conclusion

Based on high-spatial-resolution observations from the 1.6 m GST at BBSO, we find a new form of flux appearance, i.e., magnetic outbreak, in the hecto-Gauss region of pore moats. Rapid emergence, explosion, and final dissipation constitutes the whole process of magnetic outbreak. Magnetic outbreak is associated with plasma upflows and EGs, and results in weak transient brightening in the upper photosphere, without chromospheric correspondence in radiation. During 6 hr observations, six events of magnetic outbreak were identified in an approximately 40″ field of view in the negative polarity region of AR 12579; their magnetic fluxes ranged from 10^{18} Mx to 10^{19} Mx, and their lifetime was around an hour. The velocity of their exploding fragments reached 2.2 km s^{-1}. The newly observed magnetic outbreak vividly describes the physical picture of convective blowup of flux tubes, and might provide the first evidence of the long-expected convective blowup.

This work was supported by the National Key R&D Program of China grant No. 2021YFA1600500, the B-type Strategic Priority Program of the Chinese Academy of Sciences (grant No. XDB41000000), the Key Research Program of Frontier Sciences, CSA (grant No. ZDBS-LY-SLH013), Yunnan Academician Workstation of Wang Jingxiu (grant No. 202005AF150025), and the National Natural Science Foundation of China (grant Nos. 12273061, 11873059, 11533008, and 12173022). T.B. and W.C. acknowledge the support from US NSF grant Nos. AGS-1821294 and AST-2108235. We are grateful to Dr. Jack Harvey for helpful discussions and valuable comments. We would like to thank the teams of BBSO and SDO in obtaining the data. BBSO's operation is supported by NJIT and US NSF AGS-1821294 grant. GST's operation is partly supported by the Korea Astronomy and Space Science Institute and Seoul National University. We particularly thank the anonymous referee for their valuable comments and helpful suggestions.

ORCID iDs

Chunlan Jin https://orcid.org/0000-0003-4763-0854
Guiping Zhou https://orcid.org/0000-0001-8228-565X
Wenda Cao https://orcid.org/0000-0003-2427-6047
Jingxiu Wang https://orcid.org/0000-0003-2544-9544

References

Ahn, K., Cao, W. D., Shumko, S., & Chae, J. C. 2016, SPD Meeting, 47, 207
Cao, W., Goode, P. R., Ahn, K., et al. 2012, in ASP Conf. Ser. 463, The Second ATST-EAST Meeting: Magnetic Fields from the Photosphere to the Corona, ed. T. Rimmele et al. (San Francisco, CA: ASP), 291
Cao, W., Gorceix, N., Coulter, R., et al. 2010, AN, 331, 636
Cao, W., Yurchyshyn, V., Yang, X., Cho, K.-S., & Wang, H. 2022, Proc. SPIE, 12184, 1218428
Centeno, R., Blanco Rodríguez, J., Del Toro Iniesta, J. C., et al. 2017, ApJS, 229, 3
Cheung, M. C. M., Rempel, M., Title, A. M., & Schussler, A. M. 2010, ApJ, 720, 233
Cheung, M. C. M., Schussler, M., & Moreno-Insertis, F. 2007, A&A, 467, 703

Fischer, C. E., Borrero, J. M., Bello González, N., & Kaithakkal, A. J. 2019, A&A, 622, L12
Fisher, G. H., & Welsch, B. T. 2008, in ASP Conf. Ser. 383, Subsurface and Atmospheric Influences on Solar Activity, ed. R. Howe et al. (San Francisco, CA: ASP), 373
Goode, P. R., & Cao, W. 2012, Proc. SPIE, 8444, 844403
Gošić, M., Bellot Rubio, L. R., Cheung, M. C. M., et al. 2022, ApJ, 925, 188
Guglielmino, S. L., Bellot Rubio, L. R., Zuccarello, F., et al. 2010, ApJ, 724, 1083
Guglielmino, S. L., Pillet, V. M., Cobo, B. R., et al. 2020, ApJ, 896, 62
Harvey, K., & Harvey, J. 1973, SoPh, 28, 61
Jin, C. L., & Wang, J. X. 2019, RAA, 19, 69
Jin, C. L., Wang, J. X., & Zhao, M. 2009, ApJ, 690, 279
Li, Q., Deng, N., Jing, J., et al. 2019, ApJ, 876, 129
Lites, B. W., Kubo, M., Socas-Navarro, H., et al. 2008, ApJ, 672, 1237
Magara, T., & Longcope, D. W. 2003, ApJ, 586, 630
Malherbe, J. M., Roudier, T., Stein, R., & Frank, Z. 2018, SoPh, 293, 4
Moreno-Insertis, F., Martinez-Sykora, J., Hansteen, V. H., & Muñoz, D. 2018, ApJL, 859, L26
Musman, S. 1972, SoPh, 26, 290
November, L. J., Toomre, J., Gebbie, K. B., & Simon, G. W. 1981, ApJL, 245, L123
Pesnell, W. D., Thompson, B. J., & Chanberlin, P. C. 2012, SoPh, 275, 3
Rempel, M. 2018, ApJ, 859, 161
Rempel, M., & Cheung, M. C. M. 2014, ApJ, 785, 90
Roudier, T., Malherbe, J. M., Gelly, B., et al. 2020, A&A, 641, 50
Roudier, T., Malherbe, J. M., Rieutord, M., & Frank, Z. 2016, A&A, 590, 121
Schrijver, C., & Zwaan, C. 2000, Solar and Stellar Magnetic Activity (New York: Cambridge Univ. Press)
Scherrer, P. H., Schou, J., Bush, R. I., et al. 2012, SoPh, 275, 207
Sheeley, N. R., Jr. 1969, SoPh, 9, 347
Shine, R., & Title, A. 2000, Encyclopedia of Astronomy and Astrophysics (Bristol: Institute of Physics Publishing), 2038
Spruit, H. C. 1979, SoPh, 61, 363
Spruit, H. C., Title, A. M., & van Ballegooijen, A. A. 1987, SoPh, 110, 115
Spruit, H. C., & Zweibel, E. G. 1979, SoPh, 62, 15
Stein, R. F., Lagerfjard, A., Nordlund, A., & Georgobiani, D. 2011, SoPh, 268, 271
Thomas, J. H., Weiss, N. O., Tobias, S. M., & Brummell, N. H. 2002, Natur, 420, 390
Wang, H., Liu, C., Ahn, K., et al. 2017, NatAs, 1, 0085
Wang, J. X., Zhou, G. P., Jin, C. L., & Li, H. 2012, SoPh, 278, 299
Wilson, P. R. 1986, SoPh, 106, 1
Wilson, P. R. 1989, PASAu, 8, 32
Zhang, J., Solanki, S. K., & Wang, J. X. 2003, A&A, 399, 755